

Micro- and Nano-NDE in the Laboratory for Acoustic Diagnosis and Quality Assurance EADQ Dresden

B. Köhler, J. Schreiber, B. Bendjus, M. Herms,
V. Melov, L. Helfen, P. Mikulík, T. Baumbach

Fraunhofer Institute for Nondestructive Testing,
Branch Lab EADQ Dresden, Krügerstrasse 22, 01326 Dresden, Germany

ABSTRACT

NDE activities at the Laboratory for Acoustic Diagnosis and Quality Assurance (EADQ) Dresden are outlined. The applied methods comprise acoustic, thermal, optical, and X-ray ones. Additionally, scanning probe methods (SPM) and scanning electron microscopy (SEM) are used. Combinations of different methods are especially effective. This is demonstrated for the coupling of an acoustic approach with SEM. For NDE on a micro- and nano-meter scale, preparation of appropriate test flaws and the verification of the NDE results turn out to be a challenge. To meet this challenge, we propose an approach based on focused ion beam technique.

Keywords: NDE, X-ray, micro mirror, SEM, SEAM, SPM, vibrometer

1. INTRODUCTION

For the development and design of micro devices, the increasing packaging density, new materials and their combination require deeper knowledge on material behavior. Appropriate methods for quality assurance are necessary, too. Though some years ago visual inspections had been sufficient to detect defects in solder and bond contacts, more sophisticated methods have become necessary till today. This is due to:

- Defects are no more visible because of technological changes (e. g. defects in ball grid arrays are hidden).
- The number of connections per device increases, hence at constant failure rates the yield would be drastically reduced.
- One of the most important reliability problems is given by the occurrence of delaminations of different types, which cannot be detected by common electrical and visual testing methods.

Micro- and nano-NDE play an important role not only for micro systems, but also for macroscopic objects. A lot of material properties are determined by features of micro scale. So, for example, micro defects can reduce the strength of bond layers as well as the quality of thin protection layers.

In going to smaller and smaller scales, the task of verifying the results by independent e. g. destructive methods becomes more and more challenging. We propose to tackle this by focused ion beam (FIB) techniques. Examples are the machining of test flaws of micro- and nano-scale and destructive evaluation of indications delivered by acoustic microscopy.

This paper discusses selected activities of our Laboratory which are undertaken in response to the new requirements. We apply acoustic, optical, and various X-ray approaches, which will be surveyed concerning methods and features. FIB capabilities and their exploitation for the verification of NDE indications and for the machining of test flaws will be shortly described. In particular, NDE for micro mirrors will be covered, especially in regard of X-ray activities and vibrometrical detection of their mechanical-dynamic behavior.

2. OVERVIEW OF METHODS FOR MICRO- AND NANO-NDE AT THE EADQ

For many applications it is worthwhile to have different NDE methods available, which can be applied alternatively and/or in combination. Table 1 lists methods which are on-hand at EADQ, including its external lab at the European Synchrotron Radiation (ESRF) facility Grenoble, together with their most essential capabilities. Of course there is an overlap. For example, X-ray tomography can be done either in the Laboratory in Dresden but also at ESRF.

Table 1. Microscopic methods available for EADQ together with their detection capabilities.

Method	Features detected	Structure size, best spatial resolution
HF-ultrasound and acoustic microscopy	changes of acoustic impedance (as delaminations, voids, inclusions)	crack width $\ll 1\mu\text{m}$, laterally $10 \dots 100\mu\text{m}$
Thermal wave microscopy (TWM)	thermal properties, micro cracks near surface	$5\mu\text{m}$
μ -Raman	internal stresses in crystalline Raman active samples, sp_2/sp_3 -content in DLC	$1\text{-}5\mu\text{m}$
Scanning electron microscopy with electron dispersive X-ray analysis (EDX)	surface topology, element distribution	10 nm
Focused ion beam imaging, μ -machining	grain orientation, surface topology	10 nm
Scanning electron acoustic microscopy (SEAM)	domains, stresses	$10\mu\text{m}$
Scanning probe microscopy, e. g. atomic force microscopy (AFM) and magnetic force microscopy (MFM)	topology, friction properties, electric and magnetic properties, (+ others)	1 nm
X-ray radiography and tomography	density distribution (voids, inclusions), processes in real-time	$\leq 1\mu\text{m}$
X-ray reflectometry, diffractometry, diffraction imaging (topography) and fluorescence analysis	stresses and strains, grain orientation (ODF), grain sizes, phase analysis, layer properties (thickness, density, roughness), dislocation densities, lattice misorientations, element content	$100\mu\text{m}$ in the Lab, $0.3\mu\text{m}$ at ESRF Grenoble
X-ray phase contrast imaging and holography	gradients of X-ray phase velocity	$\leq 1\mu\text{m}$
Vibrometry	displacement and velocity of surface motion, near surface defects	laterally $10\mu\text{m}$, displacement $< 1\text{nm}$
Optical microscopy	optical surface properties	$1\mu\text{m}$

Loading tools (tensile and bending modules) can be attached to or implemented into the analytic devices as AFM, SEM, SEAM, thermal wave microscope and X-ray diffraction, imaging and tomography equipment. These modules load small samples high enough to investigate their elastic and plastic properties. By electronic control it is possible to impose load cycles to fatigue the samples. Most importantly, the samples can be loaded and unloaded while observing their behavior within the microscopes or X-ray facility (in-situ). The bending module is shown in Fig. 1.

The resolution of the methods given in Table 1 and the sizes of the smallest detectable features are usually very dependent on the measurement parameters as material properties, surface conditions etc.. So the given values are only for orientation and must not be considered as an exact limit.

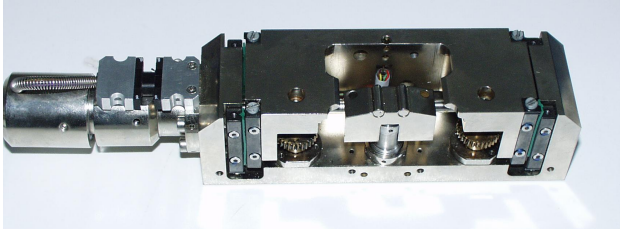


Fig. 1. Bending module for loading small samples while they are observed in microscopic tools.

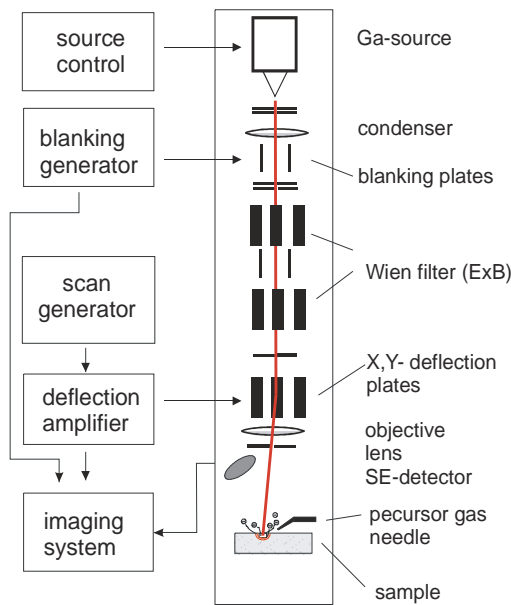


Fig. 2. Column of a focused ion beam device.

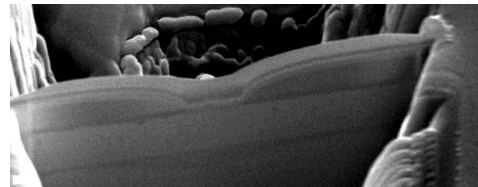


Fig. 3. TEM (Transmission Electron Microscopy) sample produced by FIB sputtering out of a part of a Micro-Opto-Electro-Mechanical (MOEM) structure. The structure is about 10 μm wide and 100 nm thick.

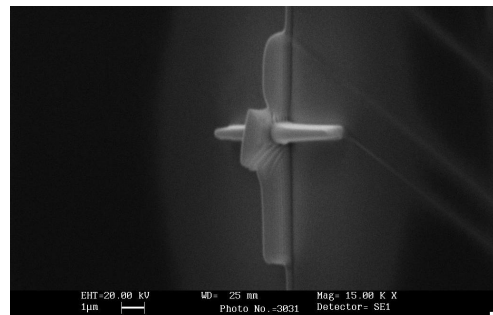


Fig. 4. Tungsten structure grown on silicon by FIB deposition out of a precursor gas. The lines are 10 μm long.

3. MACHINING AT MICRO- AND NANO-SCALE FOR NDE

All NDE methods rely on the verification of their capabilities. On the macroscopic scale this is in general not difficult: test flaws can be produced easily and flaw indications can be evaluated by destructive methods as cutting, grinding etc.. For NDE on a micro- or nano-scale the same need exists but is much more difficult to meet. As test structures, usually, regular patterns are used. For some material types they are available, however, there are specific materials for which test

structures are missing. Even for some critical NDE tasks the test flaws have to be incorporated into samples which are identical to the original parts or structures. Structuring by laser can perform this task to some extent, but the smallest achievable lateral resolution is limited by the wavelength, besides some other practical restrictions. With laser machining, smallest achievable test flaws reach some tens of a micrometer.

We propose to use focused ion beam techniques for machining surface features like grooves or notches into nearly all materials that can be exposed to vacuum. Figure 2 shows a scheme of a FIB column. It works similar like a scanning electron microscope. But instead of electrons, ions (usually gallium) are emitted by the source on the top of the column. They are accelerated and can be focused on a spot of some nm by electrostatic fields. Scanning and writing are possible, too. Compared with electrons, ions exert a stronger impact on the surface. Effects such as implantation, swelling, and material removal by sputtering occur. From the μm - down even to the nm-scale, material can be deposited in a structured way using pre-cursor gases. These gases are launched by a needle locally into the region of interest. They are cracked by the ions. This type of machine is widely used in the microelectronic industry as a sample preparation tool for SEM and TEM based defect analysis (see Figures 3 and 4 for examples of FIB machining).

4. ACOUSTIC IMAGING OF DLC LAYERS AND VERIFICATION OF THE FINDINGS BY FIB

The hardness of the surface layer plays an important role in applications where wear is an issue. A gear tooth is a good example. As in similar applications the deposition of various hard layers is attempted to improve surface hardness without losing the toughness of the whole sample. In all these applications, the binding of the layer to the surface and the quality of the layer are especially important. These properties have to be evaluated nondestructively. Acoustic microscopy is suitable for this purpose in many cases.

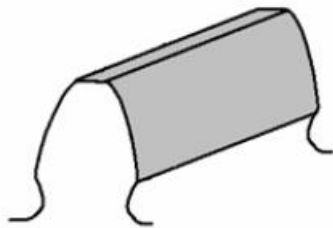


Fig. 5. Scheme of a gear tooth covered with a diamond-like carbon layer¹.

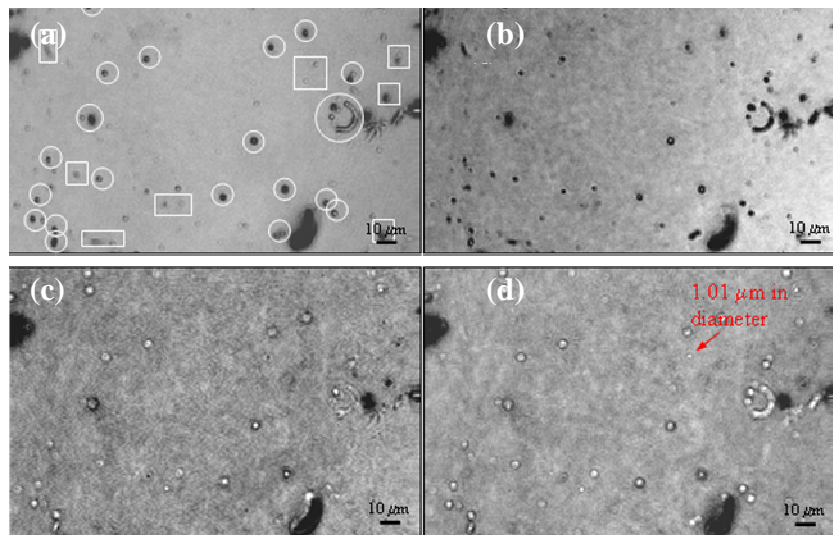


Fig. 6. Acoustic microscopy images taken at a frequency of 1.3 GHz with varying defocusing a) 0 μm , b) -2 μm , c) -4 μm , and d) -6 μm . The field view of the images was 200 $\mu\text{m} \times 130 \mu\text{m}$. Circles indicate sub-surface defects whereas rectangles mark surface features.

Figure 6 gives four acoustic microscopy images, which were taken from the side of a DLC layered gear tooth and at an identical position with increasing focal depth. By careful evaluation, surface features can be distinguished from sub-surface ones and even the depth of the latter can be estimated¹. In image (a), the sub-surface features are encircled. Their average depth is estimated as about 2 μm , using a method which is not well established, however. Hence, an independent verification of this result is heavily required. We used FIB milling to perform this verification.

Figure 7 shows the original surface and three milling steps. Two spots appear (see arrow) in such an area where the new surface is 1.4 μm below the original one. After 2.4 μm milling a third spot appears which is assumed to be an additional void. So the prediction of acoustic microscopy could be confirmed. An even more precise determination of the depth position of individual features is possible by milling of cross sections. For that a box nearby the feature position is milled, followed by a polishing step for the sidewall until the feature is crossed. Then the size, shape and position of the feature can be imaged and measured by SEM. Figure 8 gives such a cross section for the same sample as depicted in Figures 6 and 7.

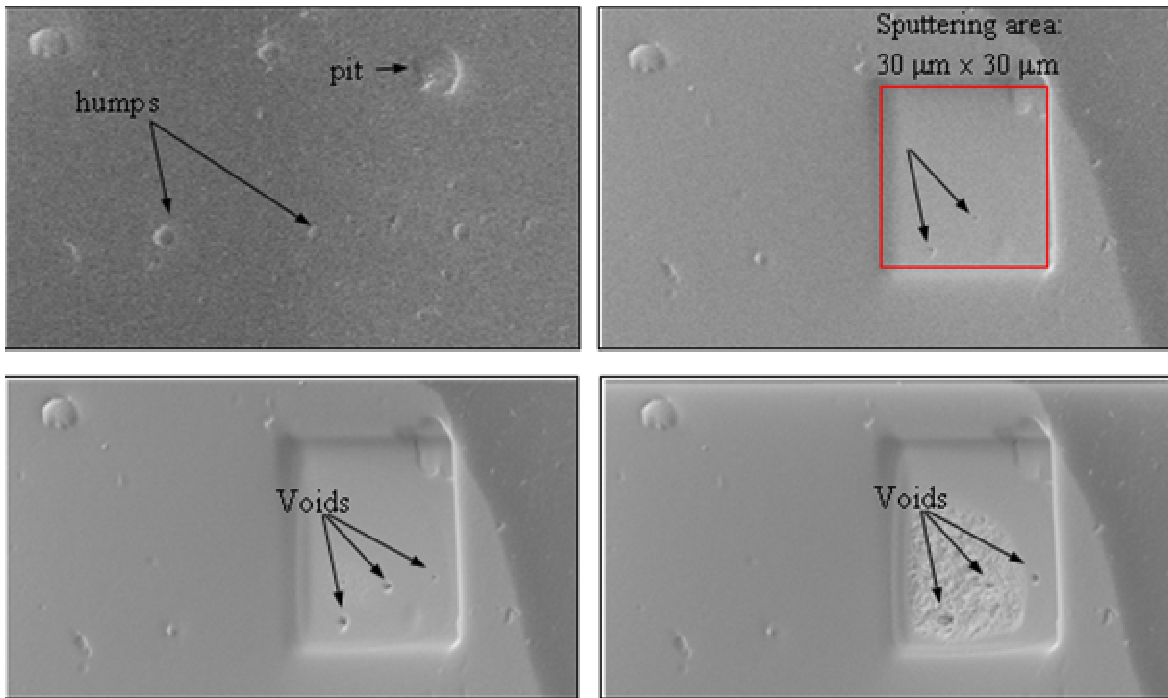


Fig. 7. SEM image of the DLC layer after four steps of FIB machining: without machining (top left), 1.4 μm removed (top right), 2.4 μm removed (bottom left) and 2.8 μm removed (bottom right).

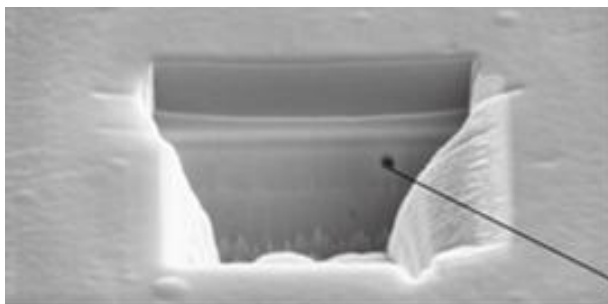


Fig. 8. SEM image of the FIB cut (groove) into the sample. Dark spot is a void.

5. TEST FLAWS FOR VERIFICATION OF AN NDE METHOD DEVELOPMENT

Tasks which combine the needs for high testing speed and for detecting flaws in small samples pose a challenge for NDE methods. Often, the components to be tested exhibit a particular - e.g. non-planar - geometry. So NDE methods must be adapted to the problem. If the product is new and the flaw rate is low (as desired), there are no test samples with typical flaws available which could serve to verify the developed NDE methods. In particular this becomes a problem for microscopic NDE due to a lack of methods for producing test flaws of appropriate size.

To be more specific, a newly designed product part of some mm size (see Fig. 10 for a detail) has to be tested in large numbers against cracks of a length down to 50 μm . Maximum testing duration was defined to some seconds per part. A special version of X-ray tomography was selected as the NDE method to be applied. For the first feasibility studies, test flaws were needed to verify the detection limit and resolution. The flaws should be machined in original samples.

Flaws of a size larger than 100 μm could be produced by applying laser methods very finely. But for smaller flaws the edge quality of laser cutting was too poor to yield satisfactory results. Therefore, FIB milling was applied. Even for the tiniest flaws of $10 \times 10 \times 10 \mu\text{m}^3$ no problem resulted. Figure 9 shows two produced test flaws of different sizes, but with typical features: (1) the side walls are very clean and precise, (2) the bottom surface is not as flat as the side walls and even more rough than the original surface, (3) the side walls form an angle which is smaller than 90° .

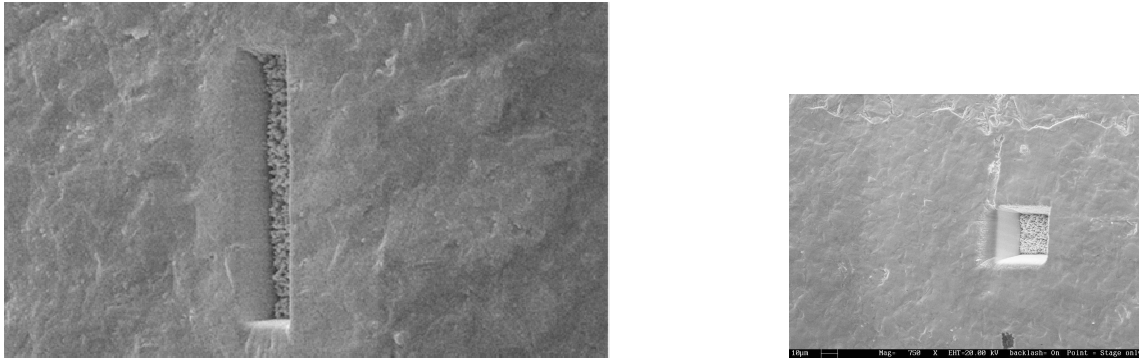


Fig. 9. SEM images of test flaws cut into the sample surface with focused ion beam technique. Left: flaw size $10 \times 50 \times 10 \mu\text{m}^3$. Right: flaw size $10 \times 10 \times 10 \mu\text{m}^3$. Viewing angle is 20° off the surface normal.

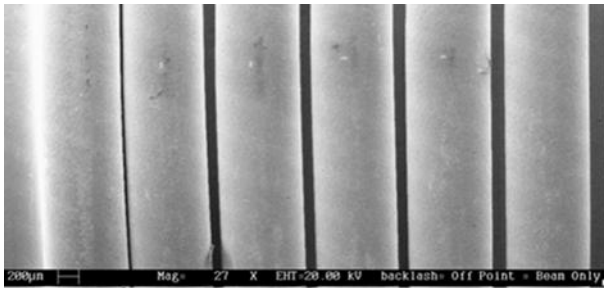


Fig. 10. Overview SEM image of a specimen part, which has to be tested for very tiny cracks; horizontal image size is 6 mm.



Fig. 11. Computer tomographic slice of a sample with a produced test flaw, which is clearly visible.

As a general rule, sputtering with normal incidence usually amplifies a small surface roughness to rather high values. This is because the sputtering effect usually increases when the surface is inclined away from the normal direction. For incident angles near to zero the sputter efficiency again drops down to zero so that no side walls can be machined normal to the surface, if no very cumbersome tilt operations are made. The remaining angle of side walls of about 3° also limits the depth of grooves of a given lateral size at the surface. It should be mentioned that the basic shape is not restricted to a rectangle but can be any one.

A variety of test flaws was produced in original samples. They were used for testing the newly developed, fast X-ray computer tomography successfully. Figure 11 shows a reconstructed slice of a computer tomographic scan in which an indication of a such a test flaw is clearly visible.

6. MATERIAL CHARACTERIZATION FOR MICROELECTRONICS AND MICROSYSTEMS

AFM and X-ray investigations focus on the structure and stability of micro-structured metallic systems (interconnections, Cu- and Al-lines for microelectronics, and components of micro-systems). In a previous publication⁴, this topic was extensively discussed. Ta-barrier layers for Cu-lines in Si-technology were thoroughly characterized³. Structural characterization of sensor materials⁹ is important to find new solutions for sensors based on micro-systems. Further details of those investigations can be found elsewhere⁵⁻⁸.

Some additional results will be reported here. Copper lines on a silicon wafer were investigated in the Magnetic Force Mode (MFM) of the AFM. The oscillating magnetic cantilever generates eddy currents in conductive samples. The resulting interactions between sample and AFM tip influence the vibrations of the tip. Thus local differences of the conductivity can be imaged by mapping the amplitude or phase signal. This way, Figure 12 (right) visualizes voids in the investigated copper lines. Another task was to check the homogeneity of Ti-layers deposited onto a 6 inch wafer. X-ray reflectivity measurements were used for that purpose (see Fig. 13).

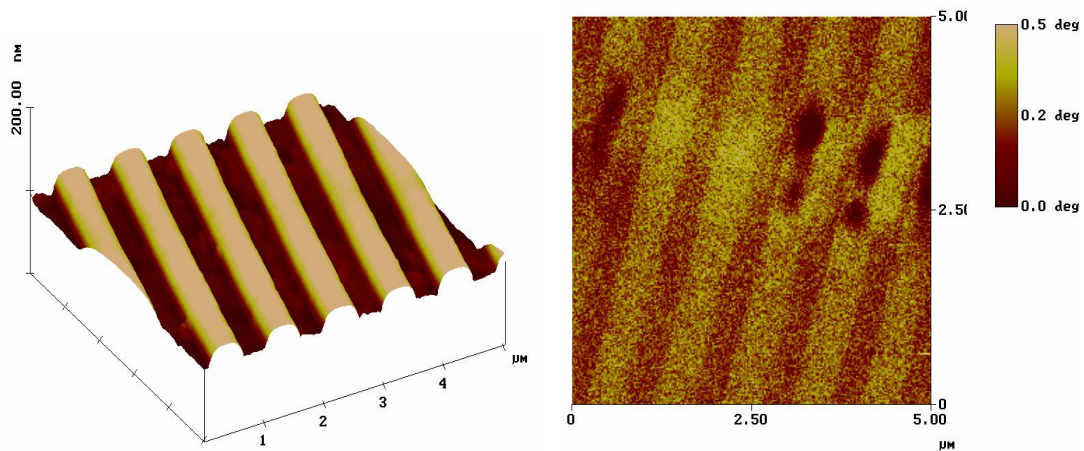


Fig. 12. AFM images of a wafer with Cu-lines (Left: topography image in Tapping mode. Right: phase image in MFM - eddy current mode). The dark fields in the right image are defects (voids), without a visible effect in the topography image.

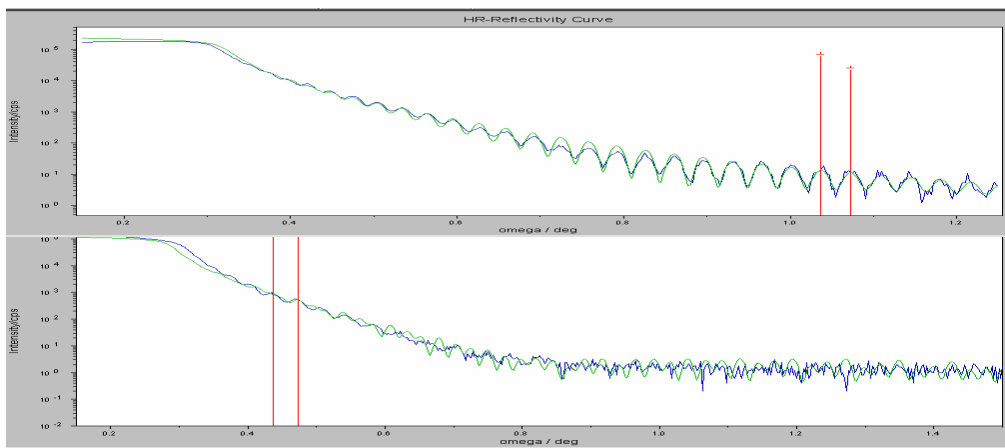


Fig. 13. Specular X-ray reflectivity curves of a Ti-layer deposited onto a Si-wafer. From the period of the oscillations the layer thickness was determined. The upper curve corresponds to the center of the wafer (thickness 118 ± 3 nm), whereas the lower one visualizes the situation for the border of the wafer (thickness about 118 nm).

In cases where laboratory X-ray equipment could not be applied to yield a satisfactory result, synchrotron radiation¹⁰ has been employed to solve the corresponding NDE task. Generally speaking, the application of synchrotron radiation for X-ray testing can supply advantages in a variety of applications. For imaging applications, highest spatial resolutions (down to $< 1\mu\text{m}$ pixel size) can be attained¹¹. Monochromatic radiation can be used to image chemical element distributions or reduce the appearance of artifacts with respect to computed tomography¹²⁻¹³. Moreover, monochromatic radiation permits the quantitative reconstruction of the linear attenuation coefficient for the selected X-ray energy¹⁴. Real-time imaging¹⁵⁻¹⁷ allows for a high temporal resolution (< 0.06 s), even in combination with monochromatic radiation and high spatial resolutions. Phase-contrast¹¹ and holographic imaging¹⁸ enable the investigation of low-contrast objects. *In situ* testing under mechanical, electric, magnetic and thermal load is facilitated to a large extent by a parallel-beam geometry.

A common problem within the scope of microelectronics is the detection of Al structures on a Si substrate. Especially, hidden structures are not detectable by light microscopy, nor can they be imaged by conventional absorption radiography since Si and Al exhibit very similar linear attenuation coefficients over a wide X-ray energy range. Figure 14 shows a phase contrast image of an integrated circuit (IC). So-called phase-contrast in X-ray radiographs results (depending on sample-to-camera distance) from diffraction at the interfaces between Al and Si which allows to image Al structures at Si substrates, especially the hidden structures. By means of holographic tomography¹⁸ low-contrast structures can be imaged quantitatively in 3D and easily separated by image processing techniques.

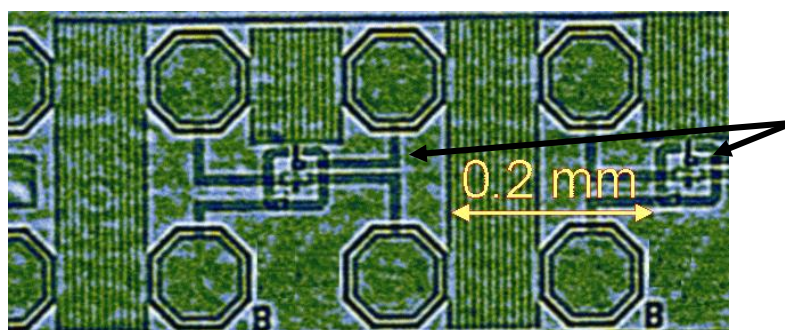


Fig. 14. Phase-contrast radiograph of an integrated circuit with Al structures at a Si substrate. Hidden Al structures on Si are not detectable by light microscopy or conventional absorption radiography but visible in the phase-contrast image (see arrows).

Besides Si-technology, the III-V-semiconductors play an increasing role in microelectronics. A comprehensive procedure how to record the spatial distribution of residual strain and stress in semiconductor single crystal wafers by scanning infrared polariscopy (SIRP) and high resolution X-ray diffraction (HRXD) is demonstrated. SIRP based on the strain-induced birefringence represents the most sophisticated method for fast lateral mapping of combinations of the in-plane strain tensor components determined in transmission of the whole wafer. HRXD adds the subsurface profile of the single tensor components of strain and stress at selected points of the wafer by analyzing sets of diffraction lines of different penetration depths calculated according to the dynamic theory of X-ray scattering. The averaged strain and stress values extrapolated from the HRXD subsurface data correlate with the corresponding results of SIRP¹⁹. Using the same method a stress analysis could be performed for Ni/C- and C/C-multilayer systems, applied for X-ray mirrors²⁰⁻²², measuring the stress gradient in the surface region of the silicon-wafer substrate.

Other investigations on crystalline semiconductor materials were accomplished by using large-area diffraction techniques at synchrotron sources. To test structural perfection of the wafers, high-resolution (in angular and in reciprocal space) X-ray diffraction imaging techniques were used with intense synchrotron-radiation. Particularly for Si, SiC, GaAs, InP wafers, defects and deformations induced by growing, cutting, grinding, etching and gluing were visualized and characterized^{23, 24}. Synchrotron topography and synchrotron area diffractometry methods allow us to analyze dislocations and lineages, micro-defects and micro-cracks, wafer tilts and warpages, tensors of local lattice rotations qualitatively and quantitatively. A method of synchrotron area diffractometry alias rocking curve imaging was developed which is based on measuring series of digital X-ray topography images at different sample orientations. Subsequent data analysis permits a mapping of local rocking curve parameters which can be interpreted as measures of local crystal quality. It

allows to reconstruct wafer perfection (e. g. for SiC wafers) by a classical full-width at half maximum approach and to measure complete 3D local lattice misorientations, Burgers vectors components or dislocations densities in the wafer^{23, 24} (see Fig. 15). This mapping can be performed with spatial resolutions ranging from e.g. 50 μm down to a few micrometer, with recent advances to micrometer-resolution imaging of local lattice tilts in overgrown GaN layers.

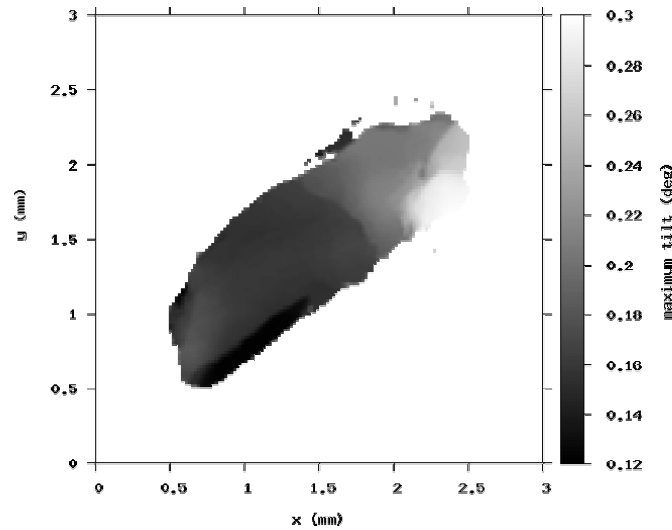


Fig. 15. Map of reconstructed maximum lattice tilt in a specific macroscopic defect in a GaAs wafer.

7. DYNAMIC BEHAVIOR OF MICRO MIRRORS

Micro-Electro-Mechanical Systems (MEMs) and Micro-Opto-Electro-Mechanical Systems (MOEMs) consist of mechanical and optical parts which have to be optimized. Their dimensions are dramatically scaled down compared to classical systems. Therefore micro-analytical methods play an important role in NDE and even more in the development process of these systems. This is true e. g. for digital micro mirrors and arrays of them. When for digital mirrors only two mirror positions (on and off) are important, any tilt angle in some range can be set up with analog micro mirrors arrays and by doing this, various gray levels can be realized. So, micro- and nano-NDE are still more important to analyze mechanical properties which influence these tilt angles. Investigations performed so far for analog micro mirror arrays include:

- microstructure inspection to determine roughness, grain size and dimension accuracy (measurements are made mainly with AFM and FIB)
- texture and grain size investigations on a local scale, mainly with X-ray diffraction
- evaluation of mechanical parameters as material stiffness and creeping by in-situ AFM imaging under thermo-mechanical load in bending tests
- evaluation of changing electrical behavior due to thermo-mechanical fatigue and drawing conclusions concerning structure changes
- X-ray residual stress analysis
- study of elasto-dynamic behavior by laser-vibrometric, microscopic measurements.

Vibration measurements shall be described in more detail. The task is to determine the mirror tilt by measuring the motion of a point at the mirror border with an accuracy better than 1 nm. The interesting time scale ranges from 1 μs (where the tilt resonance occurs) to seconds (dependence of drifts on mechanical load). For the measurements a commercial vibrometer was coupled to a microscope (see Fig. 17), so the laser spot could be positioned at the border while being observed through the microscope. The positioning accuracy was about 2 μm , which was sufficient for these investigations.

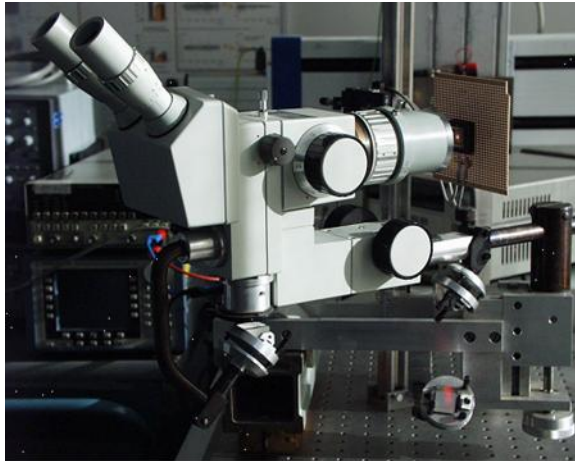


Fig. 17. Photo of the microscope, the interferometer beam is coupled through the microscope optics

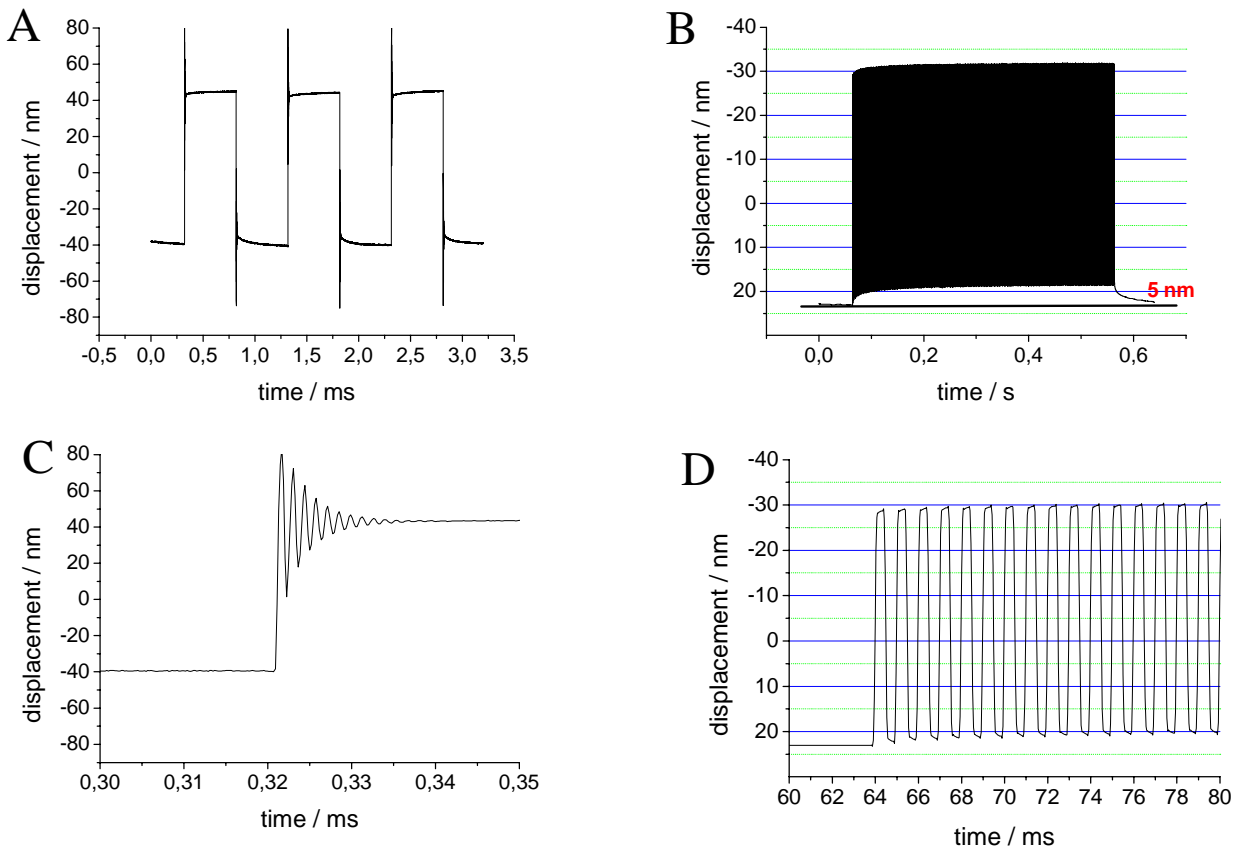


Fig. 18. Displacement at the rim of a micro mirror for various time scales.

Figure 18 illustrates the capabilities of this method by some representative results. In all examples a rectangular exciting pulse with a duty ratio of 50% was applied, switching the mirror between two tilt positions. Shortly after the electrical “switch”, there was a large spike in the mechanical answer (A). Detailed investigations with higher time resolution (C) revealed that this spike corresponds to the resonance of the mirror. It can be seen that the mirror vibration is damped out fairly well after 10 μ s, an important information for mirror development. Nevertheless, there is another slight displacement change (increase after “switch on” and decrease after “switch off”). Although strange, this behavior seems to be typical for the investigated mirrors. Its magnitude can be influenced to a large extent by the choice and treatment of the materials used for the mirrors and their hinges. Figure 18 B and D reveal yet another type of novel mechanical behavior. It can be seen in the difference of the mirror position between zero level (just constant level, mirror was not moved for a longer time) and starting to be switched between zero level and another one. In the second case, there is some kind of drift accumulation to a length of about 5 nm. When the mirror is hold again at zero, it comes back to its initial state just in some hundred milliseconds. Although not fully understood, this effect depends on material properties too and can be influenced by proper choice of corresponding treatment.

8. SCANNING ELECTRON ACOUSTIC MICROSCOPY

The combination of scanning electron microscopy with an acoustic detection constitutes scanning electron acoustic microscopy. Compared with many other particle/photo acoustic methods, SEAM offers the advantage of microscopic resolution. Figure 19 describes the measurement scheme of SEAM. It consists of a complete SEM supplemented with some additional components. These add-on’s are: beam blanker plates including amplifier for the blanking voltage, a pulse generator, a lock-in amplifier and an acoustic sensor including preamplifier. The generation of the signal takes place, as for many other particle/photo-acoustic-methods P(h)AM, by periodic excitation and signal recovery via lock-in. Then the lock-in output is fed into the auxiliary input of the SEM imaging system. So, automatically, the acoustic signal is imaged.

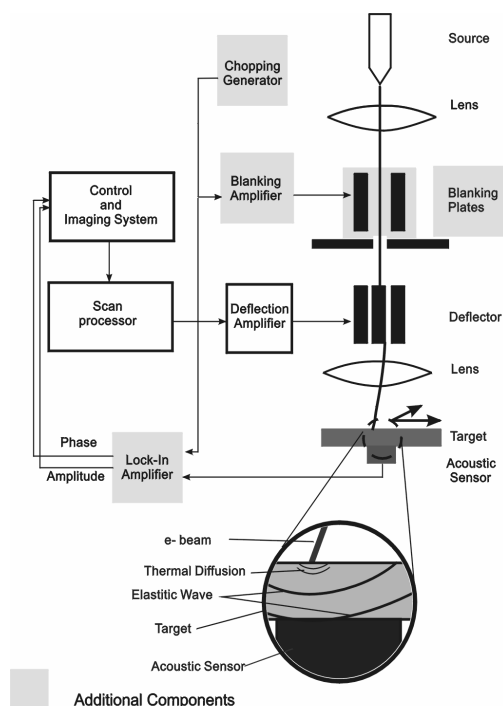


Fig. 19. Measurement scheme of scanning electron acoustic microscope; the parts which are supplements to a conventional scanning electron microscope are underlined with gray boxes.

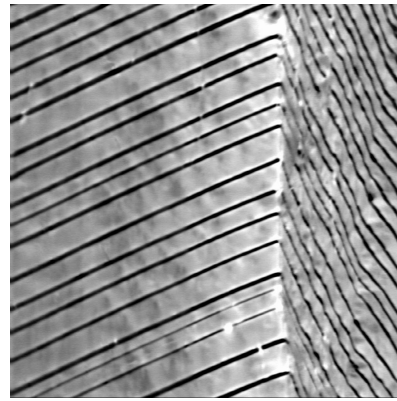
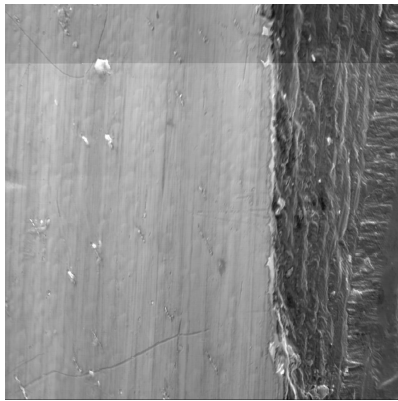


Fig. 20. Images of an edge of a bariumtitanate single crystal (magnification 150x, image size about 800 x 800 μm). Left: conventional SEM image (30 kV) taken with secondary electrons. Right: scanning electron acoustic image (SEAM).

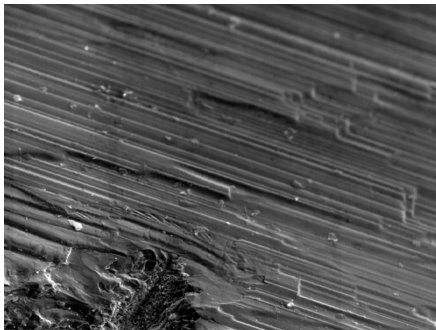


Fig. 21. Images of a disturbed part of a bariumtitanate single crystal (magnification 150x, image size about 800 x 800 μm). Left: conventional SEM image with secondary electrons. Right: SEAM with $f = 119$ kHz.

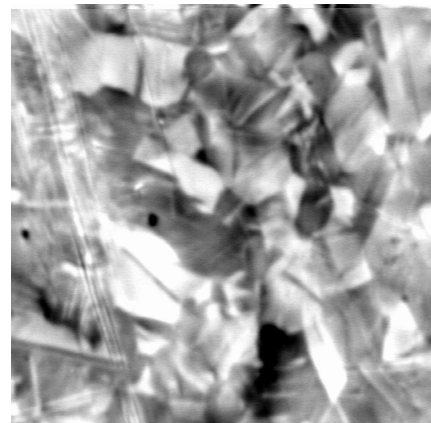
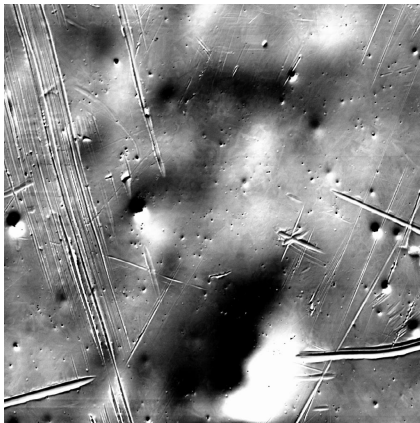


Fig. 22. Images of an austenitic steel sample with formation of martensite (magnification 200x, image size 560 x 560 μm^2). Left: conventional SEM image with back-scattered electrons. Right: SEAM with $f = 184$ kHz.

Usually the signal is very small due to the low amount of energy which can be inserted into the system by the electron beam. In regard of the excitation frequency, it is a good idea to use one resonance of the acoustic pick up system consisting of the specimen and the acoustic sensor. This frequency is usually in a range from several tens to several hundreds of kHz. An overview of possible source mechanisms is given elsewhere²⁵.

Featuring material characterization by SEAM, Figure 20 compares a SEAM image for a bariumtitanate single crystal with a simple SEM image of the same area. SEM obviously visualizes only topology contrast. In the SEAM image this topology is much less pronounced whereas marked stripes occur. The obvious explanation is that the ferroelectric domains are imaged via the piezoelectric effect.

Figure 21 shows two images of a mechanically damaged part of a crystal. Here SEAM provides a lot of the topology features which can be seen in the SEM image, with somewhat reduced resolution. Additionally, it contains a linear structure (see arrows). This can be attributed to a crack which is located totally sub-surface or nearly closed at the surface.

The third specimen is a sample of austenitic steel with some content of martensite. Again, SEM provides only information about the topology whereas SEAM goes beyond. In Figure 22, SEAM reveals the grain structure by contrast. This can be explained by the common thermo-elastic mechanism, because grains are usually anisotrop, also in their thermal and thermo-elastic properties. Figure 23 contains areas (see arrows) looking like domain structures. This is surprising because the martensite has no ferroelectric but ferromagnetic domains.

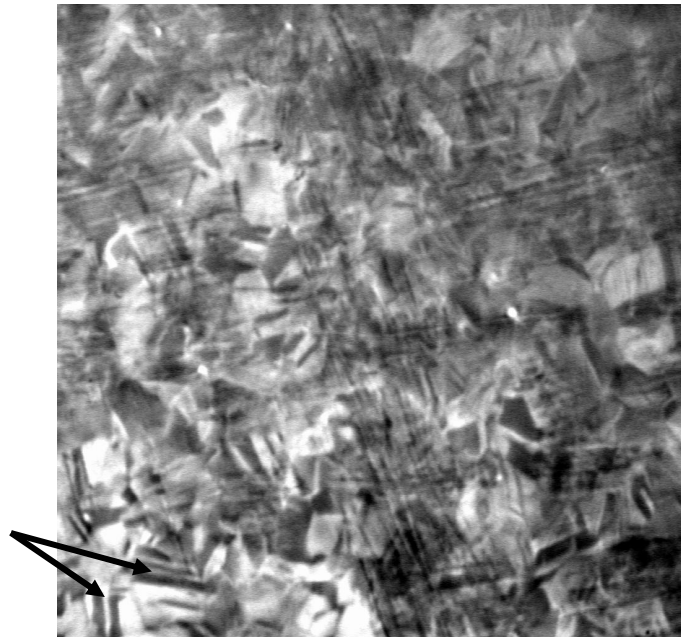


Fig. 23. SEAM image of an austenitic steel sample with formation of martensite (image size 1120 x 1120 μm^2), $f = 184$ kHz, the arrows indicate areas looking like domain structures.

The capability of SEAM to image features like sub-surface cracks and grain orientation was proven. There is evidence that the ferroelectric and ferromagnetic domain structures can be imaged too. To check this, SEAM measurements should be complemented by measurements with electric and magnetic force microscopy. All examples given prove the major advantage of SEAM to need no special surface preparation of the samples.

9. SUMMARY

Micro- and nano-NDE facilitates solving problems in both fields: miniaturized functional structures like MEMs and MOEMs but also for macroscopic components such as a gear tooth covered by a diamond like carbon layer. It is an important advantage to have a wide range of methods available. So, the most appropriate method can be selected, it is possible to apply more than one method if necessary and - as demonstrated - a combination of different methods can give completely new information.

Several examples show that NDE is not only necessary for quality control in production but gives valuable information during the product development process, especially in concern of micro-components.

REFERENCES

1. D. Fei, D. A Rebinsky, P. Zinin, and B. Köhler, "Imaging defects in thin DLC coatings using high frequency scanning acoustic microscopy", in: Review of Progress in Quantitative Nondestructive Evaluation, D.O. Thompson and D. E. Chimenti Eds., **23**, pp. 976-983, Plenum Press, New York, 2004.
2. P. V. Zinin, S. Berezina, D. Fei, D. A Rebinsky, R. M. Lemor, E. C., Weiss, C. Arnaud, W. Arnold, B. Koehler, "Detection and Localization of Subsurface Defects in DLC Films by Acoustic Microscopy", in: *2003 IEEE Ultrasonic Symposium Proc.*, M. Levy, S. C. Scheider and B. R. McAvoy Eds., IEEE, New York, in print.
3. E. Wieser, J. Schreiber, C. Wenzel, J. W. Bartha, B. Bendjus, V. Melov, M. Peikert, W. Matz, B. Adolphi, D. Fischer, "Modification of Ta-based thin film barriers by ion implantation of nitrogen and oxygen", *Proc. of Int. Conf. on Advanced Metallization and Interconnect Systems for ULSI-Application*, M. Gross, Th. Gessner Eds., pp. 257-263, Pittsburg/USA, 1999.
4. J. Schreiber, St. Braun, A. Gatto, and H. Schenk, "Testing, Reliability, and Application of Micro- and Nanomaterial Systems", presented at SPIE conference 5392 (San Diego, March 2004), this volume, paper 5392-18.
5. J. Schreiber, B. Bendjus, B. Köhler, V. Melov, and T. Baumbach, "Materials characterisation of microdevices", presented at SPIE conference 5045 (San Diego, 2003), published in this volume, paper 5045-18.
6. B. Bendjus, B. Köhler, V. Melov, J. Schreiber, "Materials Science and Testing Issues in Developing Microstructured Metallic Systems", *Proc. of Materials Week*, p. 387, 2002.
7. A. Panin, A. Shugurov, J. Schreiber, "Fractal analysis of electromigration-induced changes of surface topography in Au conductor lines", *Surface Science*, **524**, pp. 191-198, 2003.
8. J. Schreiber, V.G. Melov, M. Herms, "Breakdown of elasticity in copper and aluminium interconnects", in: *Proc. of 3rd Intern. Micro Materials*, B. Michel, T. Winkler, M. Werner and H. Fecht Eds., pp. 679-682, dpp goldenbogen, Druckhaus Dresden, 2000.
9. O. Berger, W.-J. Fischer, B. Adolphi, S. Tierbach, V.G. Melov, J. Schreiber, "Studies on phase transformations of Cu-Phthalocyanine thin films", *J. Mater. Science: Mater. Electronics*, p. 331, 2000.
10. T. Baumbach, V. Hönig, L. Helfen, D. Lübbert, "High resolution quality inspection for microelectronics and packaging by X-ray scattering and imaging techniques using synchrotron radiation", *Systemintegration in Micro Electronics*, Reichl, H. Ed., pp. 125-131, Nürnberg, 2000.
11. T. Baumbach, L. Helfen, J. Banhart, H. Stanzick, P. Cloetens, W. Ludwig, J. Baruchel, "High-Resolution Radioscopy and Tomography for Light Materials and Devices", 15th World Conference on Non-Destructive Testing, Rom, October 15.-21, 2000.
12. L. Helfen, T. Baumbach, H. Stanzick, J. Banhart, A. Elmoutaouakkil, P. Cloetens, "The Early Stage of Metal Foam Formation, studied by Computed Tomography using Synchrotron Radiation", *Advanced Engineering Materials AEM* **4**, pp. 808-813, 2002.
13. L. Helfen, H. Stanzick, J. Ohser, K. Schladitz, P. Rejmankova-Pernot, J. Banhart, T. Baumbach, "Investigation of the Foaming Process of Metals by Synchrotron-Radiation Imaging", *Proceedings of SPIE NDE/SS*, **5045**, pp. 254-265, 2003.
14. L. Helfen, F. Dehn, P. Mikulík, T. Baumbach, in: *Nanotechnology in Construction*, P. Bartos, J. Hughes, P. Trtik, W. Zhu Eds., Special Publication **292**, ISBN 0-85404-623-2, pp. 89-106, 2004.
15. J. Banhart, H. Stanzick, L. Helfen, and T. Baumbach, "Metal foam evolution studied by synchrotron radioscopy", *Appl. Phys. Lett.* **78**, pp. 1152-1154, 2001.
16. J. Banhart, H. Stanzick, T. Baumbach, L. Helfen and K. Nijhof, "Real-time investigation of aluminum foam sandwich production", *Advanced Engineering Materials* **3**, 407 (2001).

17. H. Stanzick, M. Wichmann, J. Weise, L. Helfen, T. Baumbach, J. Banhart, "Process Control in Aluminum Foam Production Using Real Time X-Ray Radioscopy", *Advanced Engineering Materials* **4**, pp. 814-823, 2002.
18. P. Cloetens, W. Ludwig, E. Boller, L. Helfen, L. Salvo, R. Mache, and M. Schlenker, "Quantitative phase contrast tomography using coherent synchrotron radiation", *Proceedings SPIE: Developments in X-Ray Tomography III*, U. Bonse, Ed., **4503**, pp. 82-91, 2002.
19. M. Herms, V.G. Melov, J. Schreiber, M. Fukuzawa, M. Yamada, "3D-Analyse von Eigenspannungen in einkristallinen Halbleiterwafern mittels Infrarot-Raster-Polariskopie und hochaufgelöster Röntgenbeugung", *Berichtsband DGZfP-DACH-Jahrestagung 2000, Zerstörungsfreie Materialprüfung*, **73.1**, Innsbruck, pp. 457-464, Berlin, 2001.
20. R. Dietsch, Th. Holz, D. Weißbach, V.G. Melov, J. Schreiber, R. Scholz, "Evolution of stress and microstructure in Ni/C multilayers used as X-ray optics in a wide energy range", *Proc. of Int. Symp. on Optical Science and Technology*, **4501**, pp. 118-126, San Diego, 29 July - 3 August 2001.
21. J. Schreiber, V.G. Melov, R. Dietsch, "Stress development in Ni/C-multilayers on Si-substrates with increasing period number", *Proc. 6th European Conf. on Residual Stresses*, pp. 797-802, Coimbra, Portugal, July 10-13, 2002.
22. R. Dietsch, A. Baranov, T. Holz, D. Weißbach, R. Scholz, V.G. Melov, J. Schreiber, "High resolution Carbon/Carbon multilayers", *Proc. of the SPIE conference on "X-Ray Mirrors, Crystals and Multilayers II"*, **4782**, pp. 160-168, 2002.
23. P. Mikulík, T. Baumbach, D. Korytár, P. Pernot, D. Lübbert, L. Helfen, Ch. Landesberger, "Advanced X-ray diffraction imaging techniques for semiconductor wafer characterization", *Materials Structure*, **9**, pp. 87-88, 2002.
24. P. Mikulík, D. Lübbert, D. Korytár, P. Pernot, and T. Baumbach, "Synchrotron area diffractometry as a tool for spatial high-resolution three-dimensional lattice misorientation mapping", *J. Phys. D: Appl. Phys.*, **36**, pp. A74--A78, 2003.
25. B. Köhler, F. Schubert, A. Peiffer, G. Hentges, "Some aspects of photo and particle acoustic methods", *Molecular and Quantum Acoustics*, **23**, pp. 225-238, 2002.